


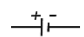
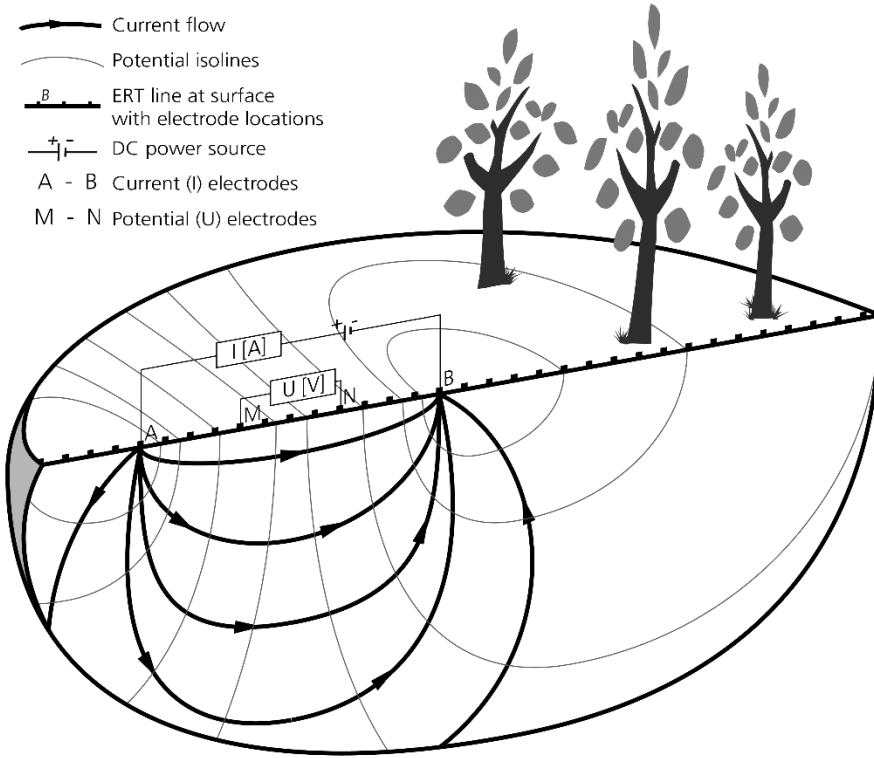


-  Current flow
-  Potential isolines
-  ERT line at surface with electrode locations
-  DC power source
- A - B Current (I) electrodes
- M - N Potential (U) electrodes



DEVELOPMENTS OF ELECTRICAL SUB-SURFACE INVESTIGATIONS THROUGH INDUCED POLARISATION

Per-Ivar Olsson

Cover figure: Schematic overview of the DCIP measurement principle for data acquisition along a line on a homogeneous subsurface. In the figure, only one pair of potential electrodes (M and N) is indicated, while it is possible to sample the potential surface with multiple potential electrode pairs at the same time. Figure adapted from the original provided by Nijland et al. (2010). (Figure 1 in the report).

STIFTELSEN BERGTEKNISK FORSKNING
ROCK ENGINEERING RESEARCH FOUNDATION

Developments of electrical subsurface investigations through induced polarisation

Utveckling av elektrisk markundersökning med inducerad polarisation

Per-Ivar Olsson

BeFo Report 191
Stockholm 2024
ISSN 1104-1773
ISRN BEFO-R-191-SE

This report is a representation of the Doctoral Thesis “Advances in time–domain induced polarisation tomography: Data acquisition, processing and modelling”.

Department of Biomedical Engineering, Lund university, 2018.

ISBN (print) 978-91-7753-851-6 ISBN (pdf) 978-91-7753-850-9

ISRN LUTVDG/(TVTG-1041)/1-167(2018)

id 387e23a8-f1f5-4f2f-8010-288f97c0e561

This BeFo report is published with the permission of the author.

Preface

When we plan and build structures below or above ground, search for suitable places for wells, or remediate contaminated areas, we need good and reliable information about the ground below. Incorrect or incomplete information about the subsurface can lead to unexpected problems. These problems can in turn lead to delays and reduced sustainability in the implementations. This report addresses how we can develop and improve the use of electrical current to investigate the subsurface.

This report is based on a doctoral thesis from Lund University and the work has mainly been performed by Per-Ivar Olsson, with advice and support from Torleif Dahlin, Gianluca Fiandaca and Esben Auken along with the participants of the reference group Nils Outters, Thomas Sträng, Roger Wisén, Christel Carlsson, Lars O. Ericsson, Malin Norin, Staffan Hintze, Andreas Pfaffhuber and Per Tengborg.

The project was financed by Formas, SBUF, Lund university, Hakon Hansson Foundation and BeFo.

Stockholm

Patrik Vidstrand

Förord

När vi planerar och bygger under eller ovan jord, när vi söker efter lämpliga platser för brunnar eller sanerar förorenade områden behöver vi bra och tillförlitlig information om marken under. Felaktig eller ofullständig information om grunden kan leda till oväntade problem. Dessa problem kan i sin tur leda till förseningar och försämrad hållbarhet hos konstruktionen. Denna rapport tar upp hur vi kan utveckla och förbättra användningen av elektrisk ström för att undersöka marken.

Denna rapport är baserad på en doktorsavhandling från Lunds universitet och arbetet har huvudsakligen utförts av Per-Ivar Olsson, med råd och stöd från Torleif Dahlin, Gianluca Fiandaca och Esben Auken tillsammans med deltagarna i referensgruppen Nils Outters, Thomas Sträng, Roger Wisén, Christel Carlsson, Lars O. Ericsson, Malin Norin, Staffan Hintze, Andreas Pfaffhuber och Per Tengborg.

Projektet finansierades av Formas, SBUF, Lunds universitet, Hakon Hanssons Stiftelse och BeFo.

Stockholm

Patrik Vidstrand

Summary

What would you find below your feet – how do you find out? Perhaps you could look at a geological map, drill, or dig? That could work, but sometimes the maps are not detailed enough, and digging everywhere to find out is impractical. Imagine if you could develop a method that allows you to see straight through the ground, as x-rays through the body! To some extent, such methods already exist; you can for example send electric current into the ground that tells you what lies beneath when it returns. The current does not see the subsurface as we do – no soil, boulders, water or bedrock – but it can tell us about its view of the underground. Its image is in terms of electrical resistivity and chargeability and can be difficult to understand if it is not translated. The translation is accomplished by comparing the electric image with, for example, geological maps and information from boreholes. With this method, we obtain more reliable and more detailed models of the subsurface. Additionally, electrical surveys can help us to determine where we need more subsurface information and where it would be most interesting to drill or dig.

When we plan and build structures below or above ground, search for suitable places for wells, or remediate contaminated areas, we need good and reliable information about the ground below. Incorrect or incomplete information about the subsurface can lead to unexpected problems. These problems can in turn lead to delays and reduced sustainability in the implementations. One example of such a project is the train tunnel through Hallandsåsen in Southern Sweden, which suffered several delays and took 23 years to complete, and its final price tag was approximately ten times the initial estimate.

This report addresses how we can develop and improve the use of electrical current to investigate the subsurface. The method has been used and developed for more than one hundred years, but bottlenecks remain that limit its use. One example is in cities where electrical installations and a complex environment in the subsurface distort the current. We then need to filter the image to make use of the results from the measurements. The method may also be limited by lack of resources needed to conduct the investigations, or to make proper interpretations of its information. By refining and optimising the method, its usefulness can be increased. For example, by enabling its use in urban areas or for projects with limited resources.

This report describes how we can process signals from electrical surveys and handle interference from other electrical installations, similar to a pair of noise-cancelling headphones. The processing allows us to retrieve more information about the subsurface and increase the reliability of the results. Another improvement that is introduced is a change of the shape of the current that is sent into the ground. The change of waveform results in a reduction in the time required for a survey, while the magnitude of the signals is increased, similar to completing a podcast in half of the time with better audio quality.

Another way to improve the method is to increase our understanding of what types of responses we can expect from the measurements. This report describes how measurement results that were previously considered erroneous can be explained, and that these are actually physically possible. By not rejecting such results, we can obtain more information from the measurements, more reliable models of the subsurface, and post-processing of the measurements is simplified. In addition, it describes how we can compensate for the effects of varying duration of current transmissions. If the effects are not considered properly, different electrical images of the same subsurface are obtained depending on whether the current is sent just one second longer or shorter.

The optimisations of the report are exemplified with, among others, results from a major survey that mapped a geologic site in terms of resistance and chargeability down to 200 metres below ground. Such information is important and can help us to take better decisions, for example in connection with infrastructure projects for a more sustainable future. Hopefully, the work in this report can increase the use of electrical surveys, ensuring we can make more informed decisions in the future.

Sammanfattning

Vad står vi på – hur tar man reda på det? Kanske man kan titta på en geologisk karta, borra ett hål eller gräva en grop? Det kan gå bra, men ibland finns det inte tillräckligt detaljerade kartor och att gräva upp allt man är intresserad av är ingen lysande idé. Tänk om man kunde forska fram en metod som gör att man kan se rakt igenom marken, som röntgenundersökningar på sjukhus! På sätt och vis kan man redan det, man kan skicka ner ström i marken som berättar om hur där ser ut när den kommer tillbaka. Ström ser inte marken som vi gör – ingen jord, sten, vatten eller berg men den kan berätta för oss om dess bild av marken. Bilden är i termer av motstånd och uppladdning och kan vara svår att förstå om den inte översätts. Översättningen görs genom att jämföra den elektriska bilden med till exempel geologiska kartor och information från borrhål. Med denna metod får vi totalt sett en säkrare och mer detaljerad modell av marken. De elektriska undersökningarna kan också hjälpa oss att avgöra var vi behöver mer information och var det kan vara som mest intressant att borra eller gräva.

När vi ska planera och bygga konstruktioner ovan eller under mark, hitta lämpliga platser för brunnar eller sanera förorenade områden behöver vi ha bra och säker information om vad marken består av. Felaktig eller ofullständig information om marken kan skapa oväntade problem. Dessa kan i sin tur leda till förseningar och minskad hållbarhet i genomförandet. Ett exempel är tågtunneln genom Hallandsåsen i Skåne som tog 23 år att färdigställa och blev cirka tio gånger dyrare att bygga än vad som först beräknats med en slutnota på över tio miljarder kronor.

Denna avhandling handlar om hur vi kan utveckla och förbättra användningen av ström för att undersöka marken. Metoden har använts och utvecklats sedan förra sekelskiftet men det finns fortfarande flaskhalsar som begränsar dess användning. Ett exempel är i städer där elinstallationer och en rörig miljö i marken förvirrar strömmen. Vi behöver då filtrera dess bild av marken för att kunna utnyttja mätresultaten. Användningen av metoden kan också begränsas av brist på resurser för att utföra undersökningarna eller för göra ordentliga tolkningar av informationen. Genom att förfina och effektivisera metoden kan den alltså vara till större nytta på fler platser och användas för att få information om marken med mer begränsade resurser.

I avhandlingen beskrivs hur man kan filtrera signaler från elektriska markundersökningar och hantera störningar från andra elinstallationer, ungefär som att sätta på den ett par brusreducerande hörlurar. Filtreringen gör att vi kan få ut mer

information om marken och ett mer pålitligt mätresultat. En annan förbättring som har utvecklats är att förändra formen på strömmen som skickas ner i marken. Formändringen gör att tiden som krävs för en undersökning halveras samtidigt som man får dubbelt så stark signal, som att lyssna igenom en podcast på halva tiden med bättre ljudkvalitet.

Ett annat sätt att förbättra undersökningarna är att öka vår förståelse för vad strömmen berättar om marken. Avhandlingen beskriver hur mätresultat som tidigare betraktats som felaktiga kan uppkomma och att dessa faktiskt är fysiskt möjliga. Genom att inte förkasta dessa resultat kan vi få ut mer information från mätningarna och säkrare modeller av marken samtidigt som översättningen av mätresultat kan bli enklare. Dessutom beskrivs hur vi kan kompensera för effekter av hur länge strömmen sänds ner i marken. Om effekterna inte hanteras får man olika elektriska bilder av samma mark beroende på om man skickar ström någon sekund längre eller kortare.

Avhandlingens förbättringar och effektiviseringar visas bland annat med resultat från en större undersökning som kartlägger geologi i termer av motstånd och uppladdning ned till 200 meter under markytan. Sådan information är viktig och kan underlätta att ta bättre beslut, till exempel i samband med infrastrukturprojekt, för en mer hållbar framtid. Förhoppningsvis kan avhandlingen öka användandet av elektriska markundersökningar så att vi kan ta mer informerade beslut i framtiden.

Table of Contents

| | |
|---|-----|
| Summary | v |
| Sammanfattning | vii |
| Nomenclature..... | xi |
| 1. Introduction | 1 |
| 1.1. Aims..... | 2 |
| 1.2. Limitations..... | 3 |
| 2. The DCIP methodology..... | 5 |
| 2.1. Resistivity | 6 |
| 2.2. Chargeability..... | 6 |
| 2.3. Waveforms | 8 |
| 2.3.1. Time-domain..... | 9 |
| 2.3.2. Frequency-domain | 10 |
| 2.4. Sensitivity..... | 11 |
| 2.5. Inversion | 11 |
| 3. Results and discussion..... | 13 |
| 3.1. Data quality and reliability | 13 |
| 3.1.1. Background drift..... | 14 |
| 3.1.2. Spikes | 16 |
| 3.1.3. Harmonic noise | 17 |
| 3.1.4. Electromagnetic coupling..... | 18 |
| 3.1.5. Bottleneck reduction..... | 19 |
| 3.2. Acquisition time | 20 |
| 3.2.1. Waveform time..... | 21 |
| 3.2.2. Sequence time..... | 21 |
| 3.2.3. Bottleneck reduction..... | 22 |
| 3.3. Data post-processing..... | 23 |
| 3.3.1. Bottleneck reduction..... | 24 |

- 3.4. DCIP survey example24
- 4. Conclusions27
- 5. Future research29
 - 5.1. Data quality and reliability29
 - 5.1.1. Anthropogenic DC noise29
 - 5.1.2. Electromagnetic coupling.....29
 - 5.1.3. Data reliability at acquisition30
 - 5.2. Survey time30
 - 5.2.1. Hardware.....30
 - 5.2.2. Dynamic waveform and protocol.....30
 - 5.3. Data post-processing.....31
 - 5.3.1. Automated data processing31
- 6. References.....33

Nomenclature

Symbols and units

| | |
|---|----------------------|
| ρ – Resistivity | (Ωm) |
| ρ_a – Apparent Resistivity | (Ωm) |
| m_0 – Chargeability | (mV/V) |
| m_{int} – Integral chargeability | (mV/V) |
| φ_{max} – MPA phase angle | (mrad) |
| τ – Cole–Cole relaxation time | (s) |
| τ_{peak} – MPA peak relaxation time | (s) |
| c – Cole–Cole frequency exponent | (–) |

Abbreviations

DC – Direct Current

CPA – Constant phase angle

DCIP – Direct Current resistivity time–domain and Induced Polarisation

EM – Electromagnetic

FD – Frequency–domain

IP – Induced Polarisation

MPA – Maximum phase angle

Rx – Receiver

SNR – Signal–to–Noise Ratio

Tx – Transmitter

TD – Time–domain

1. Introduction

The need for detailed information of the subsurface is increasing, owing to city expansion, infill projects, subsurface construction (such as tunnelling), and environmental projects (such as contaminant remediation). One common method for acquiring this geo-information is the direct current resistivity and time-domain induced polarisation (DCIP) method, which measures the electrical resistivity and chargeability of the subsurface (Dahlin, 2001; Loke et al., 2013). This report summarises selected work on developing and increasing the usefulness of the DCIP method by reducing bottlenecks and focusing on the induced polarisation part.

Electrical resistivity tomography (ERT) has been successfully used in a wide range of subsurface applications (Loke et al., 2013) such as environmental and engineering (Auken et al., 2014; Dahlin et al., 1999), hydrogeological (Auken et al., 2006; Fetter, 2001; Leroux and Dahlin, 2005) and archaeological (Argote-Espino et al., 2013; Florsch et al., 2011) projects. However, different subsurface materials can have the same resistivity (Glover, 2015); thus, it is not possible to differentiate them when only using the resistivity information. This makes induced polarisation information especially valuable, because it can be measured simultaneously with the resistivity with little or no extra effort, and materials can have the same value for resistivity but different values of chargeability. Hence, having two parameters reduces the ambiguity when relating the DCIP measurements to processes and geology. This reduction in ambiguity has been demonstrated in several applications, such as landfill mapping (Dahlin et al., 2010; Leroux et al., 2007), lithology mapping (Kemna et al., 2004; Slater and Lesmes, 2002) and microbial activities (Slater et al., 2008),

The induced polarisation phenomenon can be further evaluated by considering its spectral information, meaning its frequency dependency. Frequency dependency is described with different models and, depending on the choice of model, additional parameters can be retrieved from the chargeability measurements to further reduce any potential ambiguity. The use of spectral IP information in engineering applications is still limited, but there are several examples of research studies where the spectral information has proven useful. For example for aquifer characterisation (Fiandaca et al., 2018; Maurya et al., 2018a; Revil et al., 2015; Slater and Glaser, 2003), mapping geochemical changes (Doetsch et al., 2015a), permafrost monitoring (Doetsch et al., 2015b) and landfill mapping (Gazoty et al., 2013, 2012b, 2012a; Maurya et al., 2017). Additionally, the use of spectral IP information in data interpretation has been shown to reduce resistivity equivalences of subsurface models (Madsen et al., 2018).

Even if different levels of chargeability information generally can be retrieved from DCIP surveys, only the resistivity parameters are often evaluated in applied engineering investigations. This has several explanations, for example: older instruments with limited capability of successfully measuring the chargeability are still in use, and knowledge of how to interpret the chargeability information could be lacking.

Another important factor is related to data quality and reliability. Because the induced polarisation measurements have much lower signal-to-noise ratios compared to the resistivity measurements, the data quality can be poor. Hence, using the data would require more time for manual filtering of the chargeability data and require more resources to make use of it. This calls for an assessment on how to improve the general quality of the acquired induced polarisation data, and for developing automated ways of data quality assessment and data filtering. This is especially the case for urban three-dimensional (3D) surveys with larger amounts of data and higher noise levels.

Spectral evaluation demands a wide time-range of chargeability information (from one millisecond to several seconds) and even higher data quality than the regular “one parameter evaluation”. Furthermore, knowledge of whether IP responses are to be considered correct or erroneous is lacking. Hence, increased knowledge regarding physically possible IP responses and smart processing of the DCIP data is needed to facilitate more widespread use of the spectral IP method.

Resource efficiency (in terms of time and costs) for spectral DCIP measurements also limits the usefulness of the method. Field measurements can require several thousands of readings, where more data stacking and longer current transmission pulses may be required compared to regular DCIP acquisition. Thus, there is a need for optimising the measurement and post-processing procedures to reduce the bottlenecks that limit the usefulness of the DCIP method.

1.1. Aims

The aim of this study is to increase the usefulness of the DCIP method by developing the data acquisition and data post-processing methodologies, for reducing the usability bottlenecks that limit adoption of the method.

Therefore, the objectives of this study are to reduce field acquisition time and costs, increase the (spectral) data information content, reliability and quality, and reduce the time and costs related to post-processing of data.

1.2. Limitations

There are numerous ways to increase the usefulness of the DCIP method, and some of these are not included in the scope of the work presented in this report. This work has not considered any combination with other field surveying or geophysical methods, and only considers the direct current resistivity and time-domain induced polarisation method. This is performed primarily with its pre-existing hardware. Additionally, the handling of electromagnetic coupling has not been considered as a part of this work, except for applying an improved field procedure (Dahlin and Leroux, 2012).

Furthermore, the work has focused on developing the time-domain measurement technique rather than its frequency-domain counterpart.

2. The DCIP methodology

DCIP measurements (Figure 1) are typically carried out by injecting current into the subsurface between two electrodes while measuring the potential between one or several other pairs of electrodes (Fink, 1990; Sumner, 1976; Zonge et al., 2005). The aim of the measurements is to acquire information regarding the electrical resistivity and chargeability of the subsurface. Information from different sub volumes of the subsurface is retrieved by repeating the measurements with different electrode combinations. With electrode combinations arranged along a line, one- or two-dimensional information of the subsurface below the line can be retrieved, depending on what combinations are used. Further, if the electrodes cover a surface area, it is possible to map the electrical properties of a 3D volume (Loke and Barker, 1996).

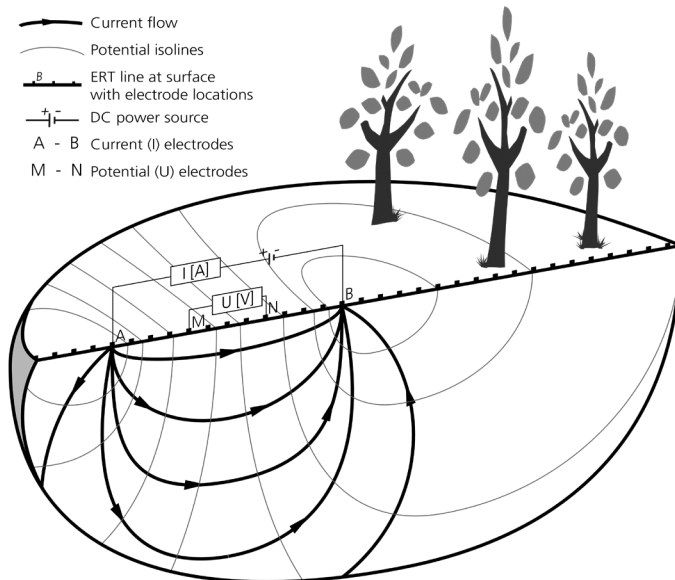


Figure 1. Schematic overview of the DCIP measurement principle for data acquisition along a line on a homogenous subsurface. In the figure, only one pair of potential electrodes (M and N) is indicated, while it is possible to sample the potential surface with multiple potential electrode pairs at the same time. Figure adapted from the original provided by Nijland et al. (2010).

2.1. Resistivity

Resistivity (ρ , unit Ωm) is a material property that quantifies to what extent a material is opposing the flow of electrical current.

From the measurements of the current (I) and potential (V_{DC}) (Figure 2), it is possible to calculate the resistance (R) of the subsurface using Ohm's law as follows:

$$R = \frac{V_{DC}}{I}$$

By also taking into account the geometry of the electrode placements (geometric factor, K), the apparent resistivity (ρ_a) can be retrieved (which only corresponds to the true resistivity of the subsurface if it is homogenous and isotropic) as follows:

$$\rho_a = K \frac{V_{DC}}{I}$$

where

$$K = 2\pi(r_{AM}^{-1} - r_{BM}^{-1} - r_{AN}^{-1} + r_{BN}^{-1})^{-1}$$

and r denotes the different distances between current (A and B) and potential (M and N) electrodes. If the subsurface has a heterogeneous distribution of resistivity, it is necessary to conduct a more advanced interpretation of the measurements to retrieve the resistivity of the subsurface (see 2.5 Inversion).

2.2. Chargeability

The chargeability (m_0 , unit mV/V) is a material property that quantifies the capacity of a material to store energy.

The chargeability is defined as the ratio between the measured voltage following a sudden change in current ($V_{IP,0}$, Figure 2), normalised with the measured potential before the current change (V_{DC}) (Seigel, 1959) from the following:

$$m_0 = \frac{V_{IP,0}}{V_{DC}}$$

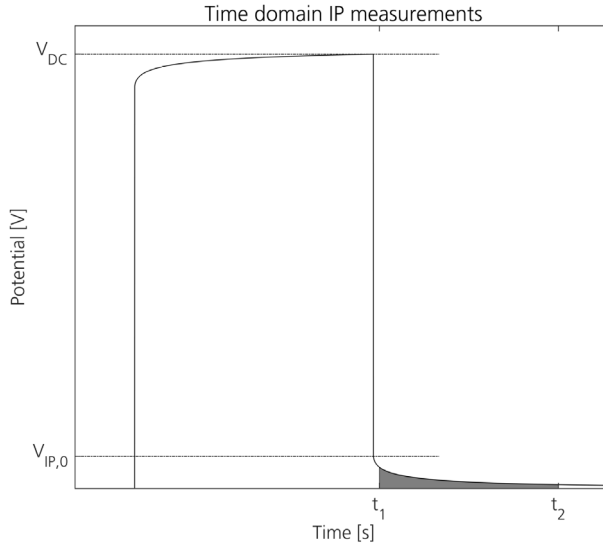


Figure 2. Theoretical full waveform potential for DCIP measurements with indication of parameters important for data evaluation.

The chargeability in the time–domain is determined by considering the transient potential response of the subsurface following a change in the injected current (Figure 2). It can be evaluated in several ways: for chargeability only (definition), for the mean chargeability within a given time interval (integral chargeability, m_{int}):

$$m_{int} = \frac{1}{V_{DC}\Delta t} \int_{t_1}^{t_2} V(t) dt$$

or for normalised integral chargeability (normalised with resistivity, see Slater and Lesmes (2002)) corresponding to surface polarisation (Binley, 2015). Furthermore, the frequency characteristics of the potential response can be considered (spectral chargeability) by using different models for describing the shape (Figure 3) of the IP response (Johnson, 1984; Tombs, 1981), for example the Cole–Cole model in the time–domain is described by (Florsch et al., 2011; Pelton et al., 1978; Revil et al., 2015):

$$V_{IP}(t) = m_0 \sum_{j=0}^{\infty} (-1)^j \left(\frac{t}{\tau}\right)^{jc} \Gamma(1 + jc)^{-1}$$

for relaxation time (τ), frequency exponent (c) and Euler's Gamma function (Γ):

$$\Gamma(x) = \int_0^{\infty} u^{x-1} e^{-u} du.$$

Analogous to resistivity and apparent resistivity, it is not possible to retrieve the chargeability model parameters of the subsurface from the DCIP measurements directly, unless it is homogenous in terms of the chargeability parameters. Therefore, inversion is normally needed. The chargeability properties are linear for small current densities used in field surveys, which typically supply less than a few amperes (below $\sim 10^{-2}$ A/m²) while non-linear behaviours have been reported for higher current densities, for example in lab measurements (Hallbauer–Zadorozhnaya et al., 2015).

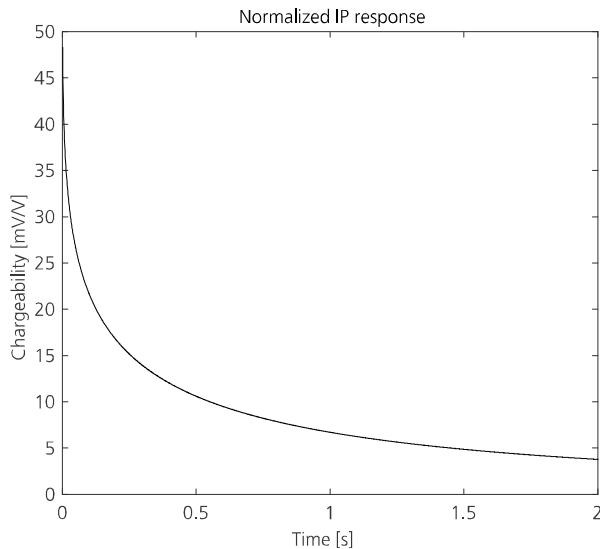


Figure 3. Normalised IP response generated from the modelled measurement seen in Figure 4.

2.3. Waveforms

The current waveform injected into the ground differs depending on whether the measurements are conducted in the time or frequency-domain. Time-domain measurements consider changes with time, while frequency-domain measurements consider at what frequencies the changes take place. The two methods are theoretically equivalent, but differ in terms of measurement and evaluation techniques (Binley, 2015).

2.3.1. Time-domain

Time-domain measurements typically inject a 50% duty cycle square current waveform as pulses of constant amplitude (Figure 4). The polarity of the current is reversed every pulse to remove background potentials superimposed on the signal measured between the receiver electrodes, caused by electrode polarisation effects (Binley, 2015). Thus, at least two pulses with opposite sign are injected. This pulse train can be repeated (stacked) to retrieve multiple readings of the potential response and to reduce the influence of noise.

The potential readings (V_{DC} , Figure 2) for calculating resistivity are taken as an average potential at the end of each current injection so that the potential has had time to stabilise as much as possible and so that the most prominent IP effects have worn off. For IP, the potential readings are taken during the current off-time and the potential is normally averaged within predefined windows, starting at a fixed delay time after the current pulses end. The time windows normally have increasing lengths (Gazoty et al., 2013) and are normally chosen as multiples of the time period of the household power grid frequency (for example 50 Hz and 20 ms in Sweden) to average out harmonic noise. The integral chargeability is determined as a weighted sum of the IP windows while, for spectral IP all windows and timing information are required for the inversion.

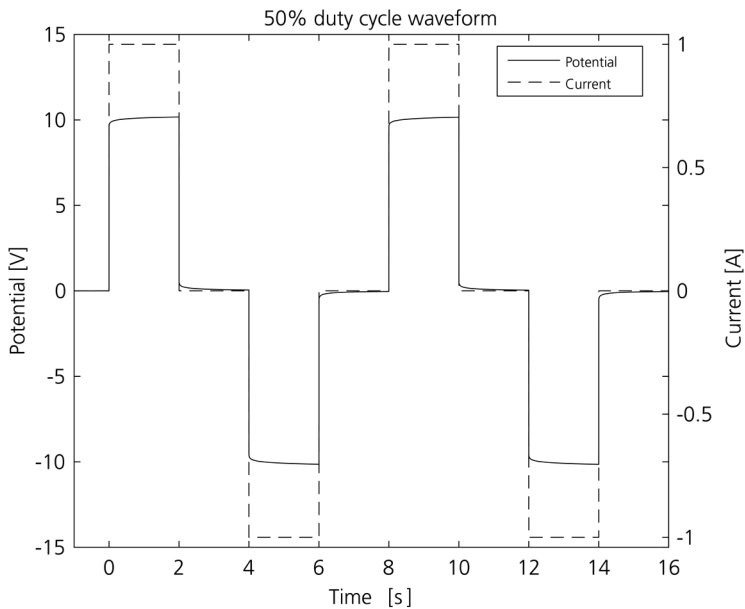


Figure 4. Injected current and modelled measured potential for the 50% duty-cycle waveform used for time-domain DCIP measurements. Two stacks are shown with four pulses and a current on-time of 2 s. The corresponding stacked, averaged and normalised IP response can be seen in Figure 3.

2.3.2. Frequency–domain

In the frequency–domain, current with a sine waveform (Figure 5) of different frequencies is transmitted, while the resistivity and IP information are retrieved as the amplitude and phase shift of the measured potential, respectively (Binley, 2015; Florsch et al., 2011). By applying a narrow passband filter corresponding to the frequency of the current transmitted, it is possible to filter out background drift (-DC), harmonic noise (by avoiding transmissions at harmonic noise frequencies or their harmonics), and partly filter the spikes. However, a recent study based on synthetic modelling and two field surveys demonstrated that it is possible to obtain qualitatively and quantitatively comparable results with the two methods, and that the TD method at present is superior in terms of acquisition time and practical spectral range in the field (Maurya et al., 2018b). The practical spectral range has been further studied in a comparison of the induction–free acquisition range for TD and FD, concluding that TD has a theoretical advantage of up to more than four decades in spectral range (Fiandaca, 2018).

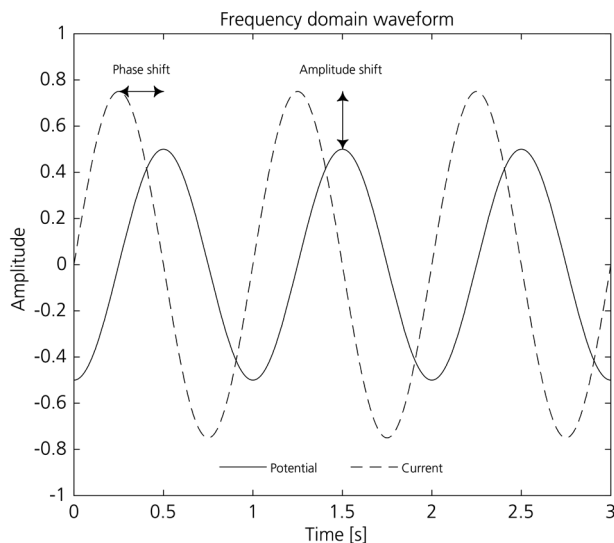


Figure 5. Schematic example of injected current and received potential for frequency–domain resistivity and IP measurements with indications of some relevant quantities. In the figure, it is assumed that the current transmission started well before time zero.

2.4. Sensitivity

Sensitivity (Figure 6) in general describes how changes in model parameters are represented in forward calculations, for example how the change in resistivity in one part of a subsurface model will change the measured apparent resistivity for a specific electrode combination (Binley, 2015). This relationship between model and DCIP data is mathematically given by the Frechet derivative, which can be solved analytically for simple models (such as a homogeneous subsurface), but it does in general require other solution techniques. For example, by parameterising and discretising the model and computing the partial derivatives numerically (McGillivray and Oldenburg, 1990).



Figure 6. Schematic example of 2D-sensitivity distribution for a homogeneous half-space and a specific electrode geometry with current electrodes A and B and potential electrodes M and N. An increase of the parameter value in a positive area (pink) will increase the magnitude of the measured quantity, while the magnitude will decrease if the parameter increase takes place in a negative area (blue).

2.5. Inversion

Inversion (Figure 7) is an iterative process that aims to find a discretised parameter model that produces synthetic measurements (forward responses) that are similar to the measurements observed in reality. During this process, the observed data is compared with the forward responses for a known distribution of model parameters (such as resistivity and chargeability), and the model parameter values are changed until the responses are similar to the real measurements (Binley, 2015; Loke and Barker, 1996; Rücker et al., 2006).

Depending on the type of parameterisation of the inversion, different numbers of parameters are used for describing the model space. For example, with the spectral induced polarisation Cole–Cole model, four parameters are used: resistivity,

chargeability, relaxation time, and frequency exponent, where the latter three describe the shape of the IP response (Fiandaca et al., 2013, 2012; Höning and Tezkan, 2007).

The time-domain resistivity and spectral induced polarisation inversion software described by Fiandaca et al. (2012 and 2013) models the current and potential waveforms, computes the forward response in the frequency-domain and transforms the response into the time-domain for comparing the measured data with the modelled response.

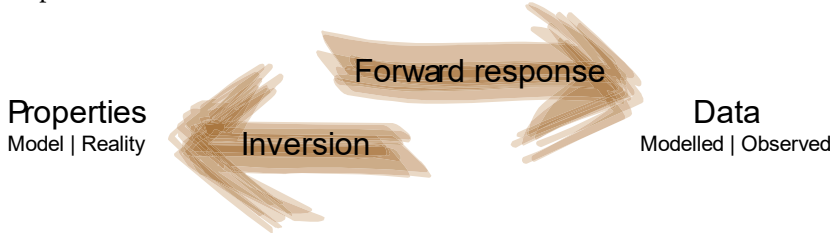


Figure 7. Schematic overview of the relationship between properties (model parameter distribution or real distribution of properties), data (modelled forward responses or observed), forward response and inversion.

3. Results and discussion

Multiple factors are limiting the usability of the DCIP methodology, and many of these are more severe in urban areas. In short, there are three main categories creating bottlenecks for DCIP usability. Firstly, issues with low data quality and reliability limit the successful use of the method in noisy environments. Secondly, the time needed for data acquisition can limit the possibilities for applying the method owing to lack of resources, especially when 3D surveys are needed. Thirdly, the post-processing of acquired data is time consuming and guidelines or knowledge on what is to be considered erroneous IP data are missing because there is a lack of knowledge of what shapes of IP responses are physically possible. This is especially relevant for spectral IP measurements and 3D surveys, both of which require more data; thus requiring more post-processing resources.

3.1. Data quality and reliability

Many technical measurement issues related to different noise sources can be avoided if the measurements are carried out in the frequency-domain instead of in the time-domain. However, frequency-domain measurements are highly time consuming compared to the time-domain (Maurya et al., 2018b) and consequently are rarely used in commercial engineering and environmental applications and are mainly used for research purposes. As this work aims to identify techniques that can be expected to be adapted for routine practical applications, it focuses on developing time-domain measurements and on pushing the limit of the available spectral IP information from direct current resistivity and time-domain induced polarisation measurements.

In field DCIP measurements, the measured potentials can be regarded as a mix of different sources (Figure 8), including the desired ground response of the current injection:

$$u_{measured} = u_{response} + u_{drift} + u_{harmonic\ noise} + u_{spikes} + u_{other}$$

To obtain an accurate determination of the potential response ($u_{response}$), it is essential to reduce or to determine and compensate for as many of the other sources as possible.



Figure 8. Different types of known sources that affect the measured potential and their typical signal characteristics: electrical fence – spikes (top left), power grid – harmonic noise (top right), tram running on DC – anthropogenic background drift (bottom left), DCIP instrument – square pulse train (bottom right).

3.1.1. Background drift

Background drift in DCIP data can originate from multiple sources, for example natural potential differences in the subsurface, natural electrode polarisation (which can be reduced using non-polarisable electrodes), and current induced electrode polarisation (if using the same electrodes for injecting current and measuring potentials). This drift manifests as a slowly changing potential trend in the full waveform potential recording (Figure 9). If not corrected, drift can corrupt both resistivity and chargeability data. However, the tail of the IP response is especially sensitive, owing to its low signal-to-noise ratio. Hence, mainly the spectral IP is affected. The correction for drift is commonly performed with a linear approximation (Dahlin et al., 2002; Peter-Borie et al., 2011).

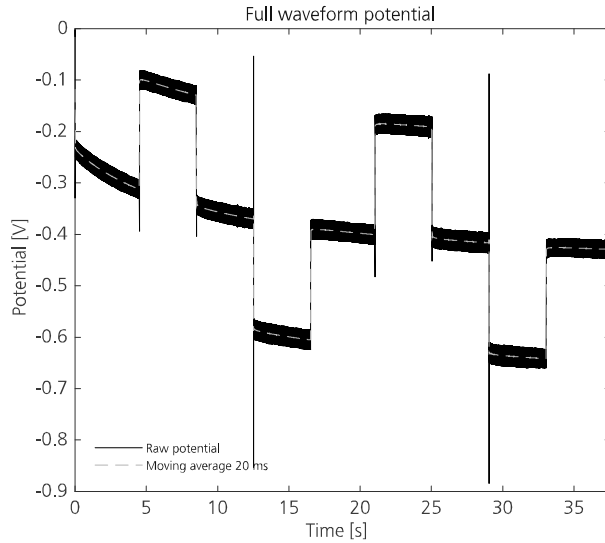


Figure 9. Example of full waveform recording that exhibits a relatively slow background variation mainly caused by current induced electrode polarisation. The full waveform is also shown with a moving average of 20 ms to suppress harmonic noise (see 3.1.3 Harmonic noise section).

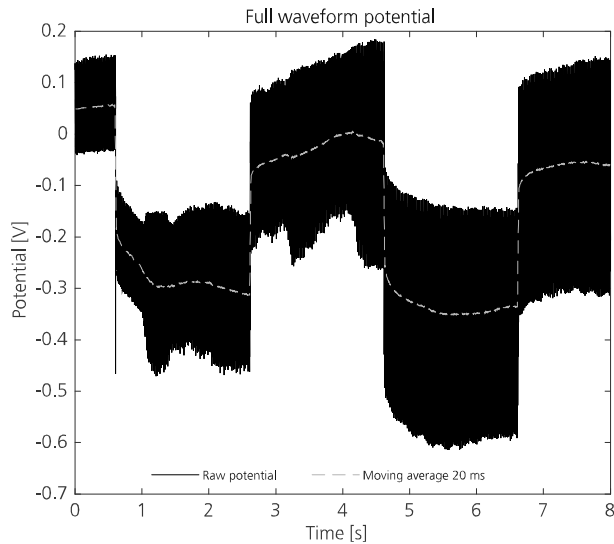


Figure 10. Example of full waveform potential recording (from a 100% duty cycle current waveform, Figure 16) that exhibits a relatively fast variation in background potential, possibly originating from anthropogenic DC noise (metro). The full waveform is also shown with a moving average of 20 ms to suppress harmonic noise (see 3.1.3 Harmonic noise section).

Another type of drift originates from anthropogenic DC sources (not related to the DCIP measurements) such as a tram, trolleybus, or metro. Such drifts are characterised by relatively fast variation, in the range of seconds (which is similar to the time range of the DCIP measurement sequence (Figure 10)). This relatively faster variation can corrupt the DCIP potential waveform readings in such a way that they become unusable, and no method has yet been found for filtering and handling such data. At present, the obvious way to deal with the anthropogenic DC noise is to conduct the measurements when the noise rate is low, for example at night, and to identify and remove corrupted measurements from the dataset (Rossi et al., 2018).

3.1.2. Spikes

Spikes originating from anthropogenic sources, such as electrical fences for livestock management, can be registered by DCIP measurements (Figure 11). These spikes can cause problems when extracting DC (resistivity). However, this particularly affects IP information from measured field data, owing to its low signal-to-noise ratio. Additionally, it should be noted that shorter IP gates are more sensitive to spikes because they consist of fewer samples.

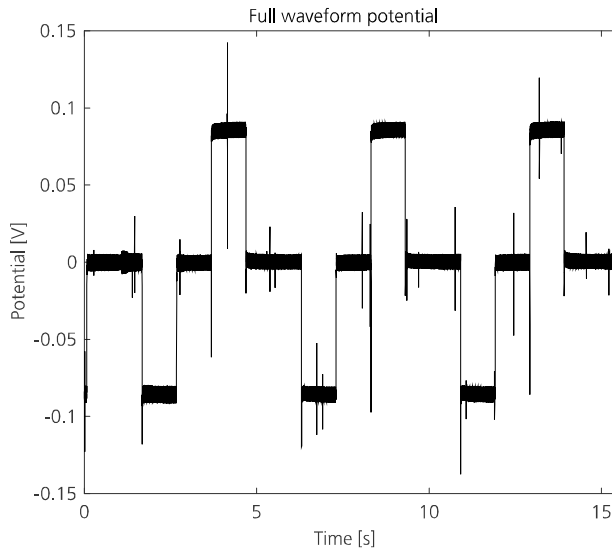


Figure 11. Full waveform potential recording with noise from electrical fences for livestock management (seen as multiple spikes).

3.1.3. Harmonic noise

Harmonic noise originates from power supply sources oscillating at a base frequency (50 Hz or 60 Hz) and its harmonics (Figure 12 and Figure 13). In DCIP processing, this is normally handled by averaging and gating over a full period of the known base frequency (for example 1/50 s or 1/60 s) for suppressing household power supply frequencies at 50 Hz and associated harmonics. However, the requirement for long gates causes a loss of early IP response information close to the current pulse change; making it more difficult to resolve spectral IP parameters (Lajaunie et al., 2016; Madsen et al., 2017). This is especially severe when conducting field measurements close to electric railways in some countries (such as Austria, Germany, Norway, Sweden, Switzerland, and USA) where the frequency of the power supplies for the trains are even lower (16 2/3 Hz or 25 Hz).

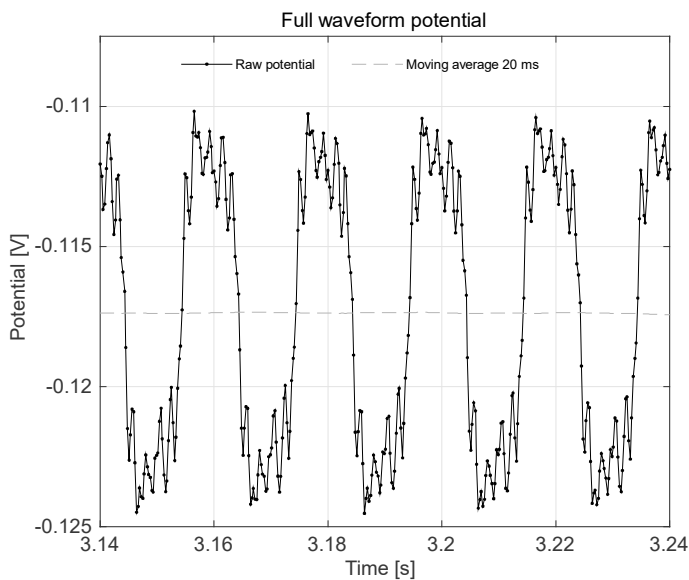


Figure 12. Excerpt of a full waveform potential recording and a moving average (20 ms window) version of the same signal. With this magnification in time, the harmonic oscillations with a main oscillation of a time period of approximately 20 milliseconds are clearly visible.

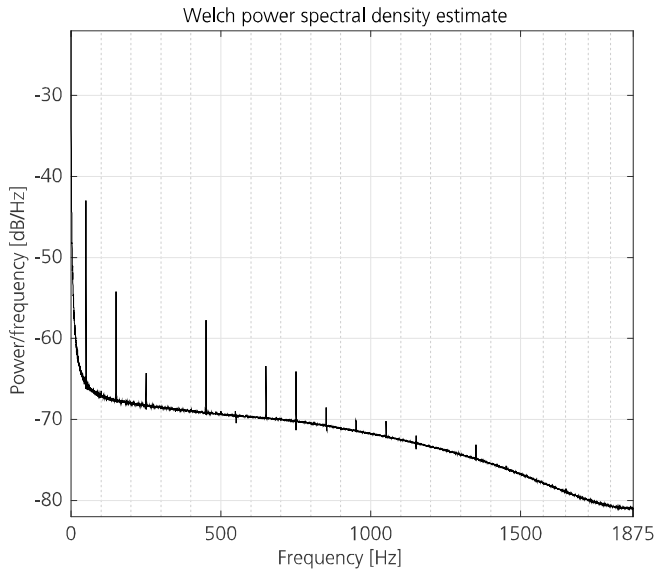


Figure 13. Welch power spectral density estimate for the full waveform potential recording seen in Figure 12 (entire signal). The periodic reoccurring energy peaks at 50 Hz and at (mainly) odd harmonics suggest that noise from a power grid is present in the signal.

3.1.4. Electromagnetic coupling

Field surveys conducted with multicore cables where the potential and current wires are bulked in the same cable (Figure 1 and Figure 14) generally suffer from different forms of electromagnetic (EM) coupling (Dahlin and Leroux, 2012). Handling of EM coupling is not a focus of this work, hence only a very brief overview is given here, but it should be noted that the coupling generally increases for longer arrays, lower resistivity, and higher frequencies (Butler, 2005).

Capacitive coupling can be defined as current leaks from high-potential surfaces or conductors to low-potential surfaces or conductors (Dahlin and Leroux, 2012). With a single multicore cable, three main capacitive couplings can occur (Dahlin and Leroux, 2012; Radic, 2004): coupling between current and potential wires, coupling between the different current wires (*A* and *B*) and coupling between the current wire and the subsurface. The main coupling effect is the one occurring between current and potential wires (Radic, 2004). One method to reduce this coupling is to increase the distance between the current and potential wires by using two multicore cables (Figure 14, top), one for current transmission, and the other for potential measurements (Dahlin and Leroux, 2012).

Inductive coupling operates through magnetic fields and thus differs in origin from capacitive coupling. It is possible to compensate for this coupling by means of

modelling and by including it in the inversion (Fiandaca, 2018; Ingeman–Nielsen and Baumgartner, 2006; Kang and Oldenburg, 2018), but because the focus of this work is elsewhere, this has not been considered in this work.

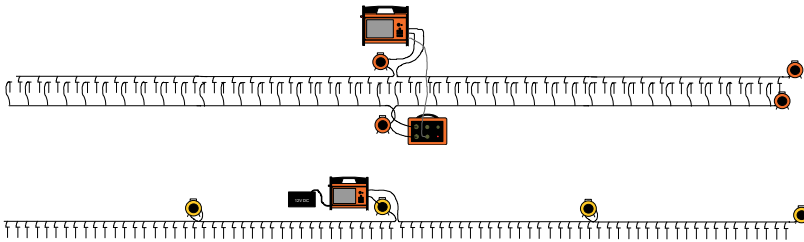


Figure 14. Example of measurement setup with two multicore cables (top). One cable and every second electrode are used for current injection while the remaining cable and electrodes are used for measuring potential. By increasing the distance between the current and potential wires, the capacitive coupling between the two is reduced. An example of the traditional setup is provided for comparison (bottom). Image adapted from original by Torleif Dahlin.

3.1.5. Bottleneck reduction

In this work, reduction of data quality bottlenecks has been achieved in two main forms. Firstly, signal levels have been increased through waveform optimisations and secondly, noise levels have been reduced by signal processing schemes. Data reliability bottlenecks have been reduced in the same manner, and with a method for data driven error estimates in terms of standard deviation (STD) (Olsson et al., 2016).

Specifically, the IP signal levels are increased by up to a factor of two by switching from a 50% to a 100% duty cycle waveform (Figure 16), and taking the IP measurements during the current injection. This causes a superposition of the IP charge–up and discharge and a theoretical doubling of the signal levels.

The noise levels are further suppressed by signal processing of recorded full waveforms (Olsson et al., 2016). This processing reduces bottlenecks by improving the handling of spikes, harmonic noise, and slower background drifts. Further, it also increases the overall SNR by introducing the use of tapered and overlapping IP gates. These improvements also double the spectral information content of DCIP data by enabling shorter gates close to the current switch as a result of removing the need for gates to be multiples of the time period of the harmonic noise (Figure 15) and by recovering a more accurate IP response shape at later times. The processing scheme also includes methods for data–driven estimation of the individual uncertainty for each IP gate based on contributions from the different noise sources and the data variability within each gate.

These improvements have been successfully applied in field surveys (for example Fiandaca et al., 2018; Johansson et al., 2017; Maurya et al., 2018; Olsson et al., 2017). However, the signal–processing scheme is applied after the DCIP acquisition;

therefore, it is not possible to use the reliability measures during field acquisition. With real time processing (with more advanced or cloud connected instruments) it could be possible to use the data quality and reliability measures to repeat failed measurements automatically, or to alert DCIP operators to possible issues, to further enhance data quality and reliability. Additionally, issues remain with faster varying background potential, such as the one generated by anthropogenic DC sources (for example metro and trams).

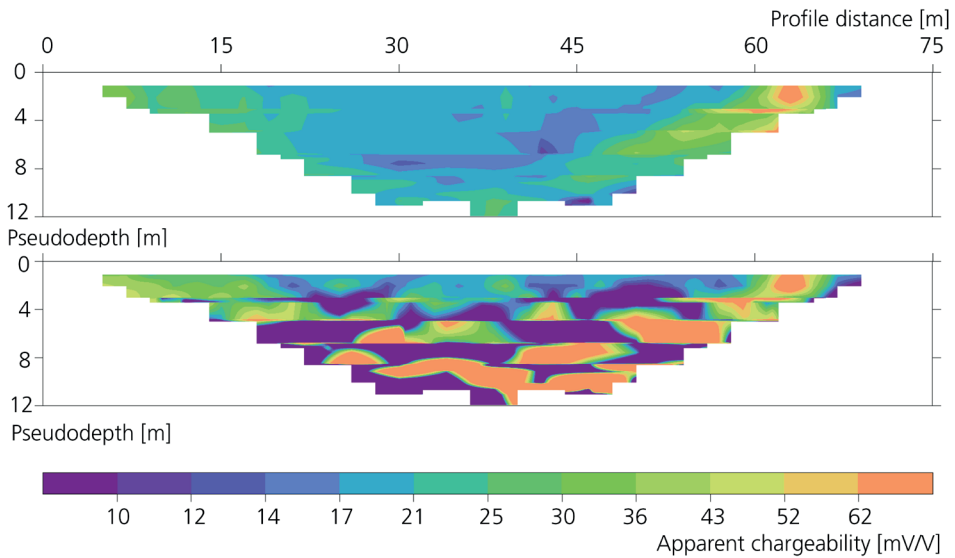


Figure 15. Pseudosections for IP gate 9 (width of approximately 5 ms, center gate time at approximately 16 ms) exemplifying the effect on data quality from full waveform processing (top) and the corresponding pseudosection with standard processing (bottom). Note that pseudosections with smooth transitions in apparent magnitude generally indicate data of good quality.

3.2. Acquisition time

The time needed for a DCIP survey can generally be divided into two parts, excluding the time related to logistics for personnel and equipment. The first part is hardware related, including time spent on positioning and aligning the equipment, installing electrodes, connecting cables, ensuring good electrode contact, and the reverse procedure at the end of the survey. The second part relates to the acquisition of the DCIP data, where the measurement instruments inject a specific current waveform into

the ground and measure potentials in a predefined sequence of electrode combinations. The focus in this work is on the second part.

For a given DCIP instrument, the time needed for the acquisition of a DCIP dataset mainly depends on two factors: the time needed for a full current injection waveform, and how many times this waveform needs to be repeated. This refers to how many and what combinations of electrodes for injecting current and measuring potentials are to be included in the dataset.

3.2.1. Waveform time

For the 50% duty-cycle waveform, the time needed for a full current injection sequence (positive and negative pulses, off-time and stacking), scales linearly with both the pulse duration and the number of stacks. For example, with 2 s pulses and two stacks, the total waveform time is 16 s (Figure 2). Doubling the stacks or the pulse duration to four would double the waveform time (32 s). Furthermore, for a given instrument, the acquisition time scales approximately linearly with the waveform time, neglecting overhead time related to instrument relay switching and transmitter setup. Some instruments, such as the ABEM Terrameter LS series, are capable of employing adaptive stacking within some predefined bounds based on the V_{DC} variance, and attempt to reduce it below a specified threshold. However, owing to superposition of potential responses from previous pulses, the theoretical V_{DC} and especially V_{IP} values are different for each pulse (Fiandaca et al., 2013, 2012). Thus, such adaptive stacking possibilities are not considered in this work.

3.2.2. Sequence time

For a specific waveform and DCIP instrument with a given number of Tx- and Rx-channels, switching capacity, and other factors, the time needed for acquiring the full measurement sequence only depends on the measurement protocol used. The measurement protocol describes which current and potential electrode pair combinations are to be measured for the dataset. The protocol is typically predefined prior to a survey and is generally optimised for resolution, SNR, lateral and vertical data density based on homogeneous half-space modelling, and on its efficiency for multi Rx-channel use (Dahlin and Zhou, 2006). Some reduction in sequence time is achieved by measuring multiple potentials with several Rx-channels, for example up to 12 for the ABEM Terrameter LS2 instrument, or by transmitting current with several Tx channels, for example up to three for the Syscal Multi-Tx instrument. The multiple Tx-technique places special demands on the transmitted waveforms, where using code-division multiple-access for separating the signals requires that any waveform pair must be mutually orthogonal (having scalar products equal to zero) (Yamashita et al., 2014).

3.2.3. Bottleneck reduction

In this work, reduction in acquisition time has been achieved by means of reducing the waveform time. Specifically, with the typically used 50% duty cycle current waveform, only half of the waveform time is available for resistivity and IP measurements. In contrast, the 100% duty cycle waveform (Figure 16) and taking the IP measurements while the current is being transmitted the full duration of the waveform are used for measurements. With numerical modelling of current waveforms with 50% and 100% duty cycles it is demonstrated that the waveforms have comparable sensitivity regarding the spectral Cole–Cole parameters (Olsson et al., 2015). Furthermore, inversion of field data acquired with both waveforms confirms the modelling results and confirms that it is possible to retrieve similar spectral Cole–Cole inversion models if the waveform of the injected current is included in the forward computations.

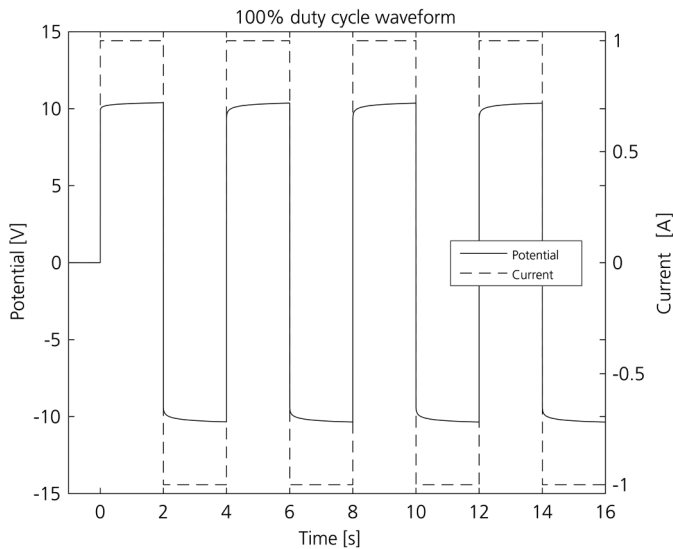


Figure 16. Injected current and modelled measured potential for a 100% duty–cycle waveform. With a pulse duration of 2 s, four stacks are achieved in 16 s compared to two stacks with the 50% duty–cycle (Figure 4). For the same number of stacks, the 100% duty–cycle would require 8 s.

Another aspect of the waveform time is related to the pulse duration and number of stacks, where the effects of varying pulse duration are discussed in Olsson et al. (2019). For short waveforms and thus acquisition time, it is desirable to use short pulse durations (and few stacks). On the other hand, it is desirable to use longer pulses (and more stacks) to improve data quality and spectral information content. Thus, there is a trade–off between data quality and acquisition time, though it is shown to be possible

to obtain similar inversion models independent of pulse duration, within almost one order of magnitude in pulse duration difference, if noise and geological conditions are favourable (Olsson et al., 2019). Furthermore, for field surveys, the waveform is typically fixed by the operator (at best), after considerations regarding expected noise conditions, chargeability magnitudes, and available resources for time spent in the field. Instead, it may be possible to determine the noise and spectral IP conditions continuously, to dynamically optimise the waveform throughout the survey based on noise levels and on the required subsurface information to decrease the acquisition time further.

The acquisition time bottleneck reductions can have a significant impact on DCIP surveys in general. This is especially true for surveys where time (and cost) efficiency and reliable data quality are important factors. Specifically, the findings are of value for DCIP surveys conducted in urban areas where the heterogeneous subsurface demands time-consuming 3D acquisitions. However, bottleneck reductions in this work have only considered waveform optimisations, while there are also possibilities for further optimisation based on sequence time. This can be achieved by reducing protocol size, or dynamically adapting it to estimated subsurface conditions instead of to a homogeneous half space (Stummer et al., 2002) or by improved hardware, for example by increasing the number of Tx/Rx channels.

3.3. Data post-processing

Here, data post-processing refers to processing of DCIP data after the measurements, but before the inversion. Such processing involves visual inspection of the acquired data; meaning plotted as pseudosections or IP responses as magnitude-vs-time plots. The purpose of post-processing is to determine which data should be forwarded to the inversion routine, and which should be considered as outliers or measurement errors. Currently, this is essentially a manual process, and it is also based on the experience and knowledge of the individual or individuals managing the processing without general scientifically based guidelines. However, recent studies have presented methods for semi-automated IP processing for integral chargeability and strictly decaying full IP responses (Flores Orozco et al., 2018; Rossi et al., 2018).

For data of excellent quality, manual post-processing can be relatively fast but post-processing of larger full IP response datasets for spectral inversion can take several days to complete. Additionally, post-processing involves largely manual labour requiring experienced and skilled personnel. Thus, practitioners may be unable to successfully use the DCIP method owing to lack of resources for post-processing, especially in low resource applications or for spectral induced polarisation inversions that require additional data post-processing.

3.3.1. Bottleneck reduction

In this study, data post-processing bottlenecks are reduced by improving the data quality and estimating its reliability, as previously described (see 3.1 Data quality and reliability section), and by increasing the knowledge on what types of IP responses are physically possible. Specifically, a basic mechanism (Figure 17) for previously disregarded IP responses is described (Fiandaca et al., 2019). Furthermore, a classification system based on the temporal development of the IP response magnitude and its derivative is introduced for seven different types. This novel knowledge and classification will facilitate decisions in the manual processing work and could reduce the required resources for this type of task. Furthermore, it could lay the foundation towards semi-automated post-processing steps to reduce the need for manual work significantly. Such improvements would be very beneficial for DCIP post-processing in general. This is especially true for large 3D datasets or data acquired in low SNR conditions (or both), as discussed in a recent study (Rossi et al., 2018) for inversion of integral chargeability data. Corresponding semi-automated processing for full response IP data could encourage and increase the use of spectral full IP response inversions.

Solely considering the integral chargeability can be misleading, and probably makes it more ambiguous when trying to relate IP models to processes and geology, or previously reported integral chargeability values. Furthermore, if the full waveform is not included in the inversion, care needs to be taken to make certain that the same acquisition settings are used when making complimentary, verification, or time-lapse measurements. This ensures that different data sets will be comparable in both the data and the model space.

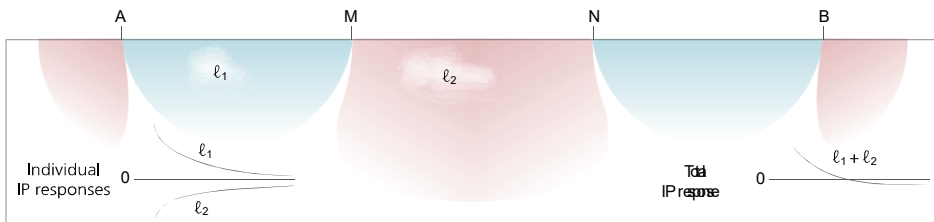


Figure 17. Schematic description of the basic mechanism for the superposition of individual IP responses (from IP anomaly regions l_1 and l_2) and the origin of non-standard IP responses ($l_1 + l_2$). Superposition of contribution from positive (pink) and negative (blue) sensitivity regions with different IP response shapes gives a total IP response crossing zero mV/V.

3.4 DCIP survey example

A large-scale DCIP survey was carried out close to Dalby municipality in Southern Sweden to map geological structures and the depth to the bedrock (Rossi et al., 2017).

Four profiles, up to one kilometre in length, were acquired in the survey, which enabled the retrieval of subsurface information to approximately 200 metres below the surface. Furthermore, the inferences from Olsson et al. (2015), Olsson et al. (2017) and Olsson et al. (2019) were used in the survey to reduce the acquisition time and to improve the data quality and reliability: 100% duty-cycle current waveform with 4 s pulses and full waveform signal processing. The results from the survey are presented in detail in Rossi et al. (2017). In general, the survey was able to map depth to bedrock and main features related to a major geological deformation zone (the Tornquist zone, trending south-east to north-west), and larger weathering zones.

Another DCIP acquisition of smaller scale (Olsson et al., 2017) which also made use of the results from Olsson et al. (2015), Olsson et al. (2017) and Olsson et al. (2019) was carried out in a quarry just north of the large scale survey. Six parallel profiles, approximately 160 metres in length (Figure 18), were acquired in the vicinity of the active quarry, which enabled detailed documentation of the bedrock in quasi-3D space as the quarry operation progressed further into the subsurface volume investigated with geophysics. The geological interpretation of the documentation shows the presence of granitic gneiss, amphibolite and diabase as well as faults, brecciated zones, clay weathering and mineralisation within the investigated volume. An amphibolite unit, which also coincides with a vertical fault and weathered zone, is seen in Figure 18 as a slightly darker area at around 30 metres from the right-hand side of the profile.

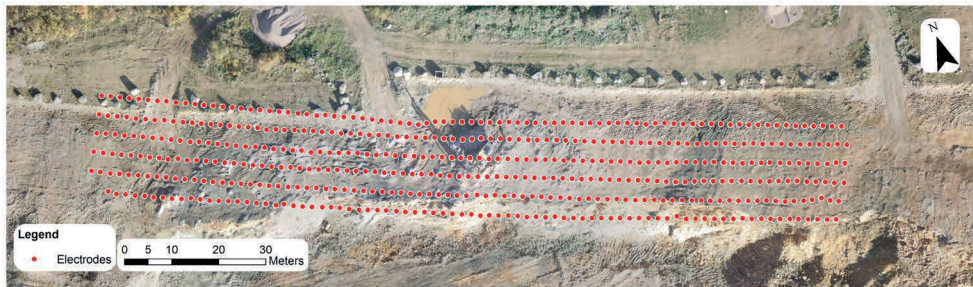


Figure 18. Overview of electrode positions together with an aerial photo taken approximately half a year after the geophysical field survey. Note that the overburden that was present during the field survey has been excavated and the slightly darker structure at approximately 30 metres from the right hand side of the profile shows the presence of amphibolite rock.

With these dense 2D DCIP profiles, it is viable to conduct a full 3D inversion of all profiles simultaneously. However, 3D inversion software that handles spectral IP, and models the transmitter and receiver waveform, is not available. Consequently, the DCIP data was inverted with standard 3D inversion software (Res3Dinv, version 3.11.62) for resistivity and integral chargeability and thus the retrieved IP parameters will not correspond to a quantitative material property (Fiandaca et al., 2019). However, the IP parameter distribution will still show qualitative differences in chargeability magnitude.

Figure 19 shows parts of the models from the 3D inversion as resistivity (top) and integral chargeability (bottom) together with a textured terrain model based on structure-from-motion and drone photography. The low-resistive zone with slightly lower integral chargeability (below 5 mV/V) on the right-hand side extends to the full depth of the model and coincides with the previously mentioned vertical fault and weathered zone next to the amphibolite. The lower resistivity in this area corresponds well with what is interpreted as weathered fracture zones in Rossi et al. (2017), though the orientation of the geophysical anomaly (south-west to north-east) suggests that it is related to another deformation zone (such as the Protogine zone).

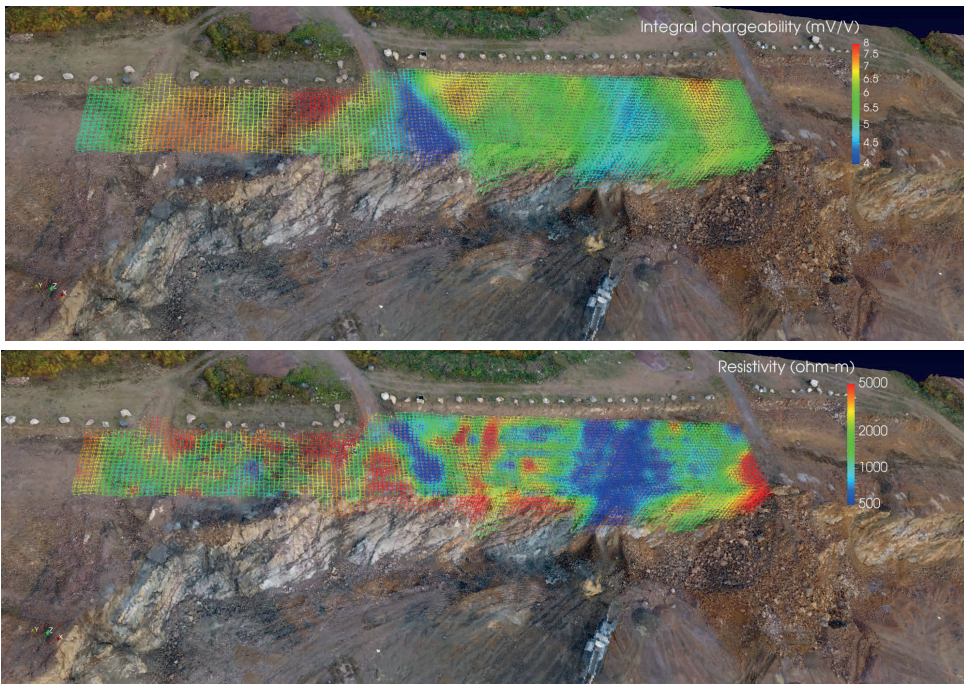


Figure 19. Visualisations of resistivity (top) and integral chargeability (bottom) inversion models together with a textured terrain model based on structure-from-motion drone photography. In the figure, most top parts of the inversion models are visible because the overburden that was present during the field survey was removed before acquiring the data for the terrain model.

4. Conclusions

The work presented in this report demonstrates that many usability bottlenecks of the DCIP method can be reduced. Specifically, field resource efficiency is increased by means of current on-time IP measurements and waveform optimisation, which speed up IP measurements and increases the SNR by up to a factor of two. Additionally, resources needed for data post-processing are reduced by improvements in data quality through a comprehensive full waveform signal-processing scheme. Data post-processing is further facilitated by increasing the data reliability through data driven error estimates, and by improving our basic understanding of physically possible responses. Furthermore, the available spectral information from DCIP surveys is substantially increased by enabling extraction of the IP response closer to the pulse than was previously possible. In combination with more accurate removal of background drift potential that can handle non-linear drift cases, the data quality is improved at late times and the spectral information content is further increased.

This work has provided tools and demonstrated their applicability for substantially increasing data quality of the spectral IP, and increasing the understanding of possible responses. However, extensive work regarding manual quality assurance and filtering of the IP response data is still required to enable successful interpretations and spectral IP inversions. Hence, there is scope for further development related to data acquisition, quality, and post-processing.

However, this work adds small but substantial contributions to the advancement and scientific understanding of the DCIP method. As such, after implementation and dissemination, it can contribute to and increase the use of the method for acquiring detailed subsurface information in applications such as construction projects, hydrogeological mapping and environmental projects. This information can hopefully lead to a more sustainable society, by enabling more informed decisions regarding the subsurface, leading to more efficient resource use and reduced risks in terms of economy, society, and the environment.

5. Future research

As indicated in previous sections, there remain many issues to be resolved for making spectral DCIP interpretation a standard tool in applied engineering applications.

5.1. Data quality and reliability

5.1.1. Anthropogenic DC noise

There are some field cases where noise sources that have a large effect on the measured potential cannot be handled by the processing routine previously described (Olsson et al., 2016). Specifically, such a noise source could be electrical vehicles running on DC (for example trams), generating a slowly varying DC offset with similar time-scale as the IP responses. Another problematic noise source can be trains running on AC passing close to a field survey, generating harmonic noise with a fast varying amplitude and phase, possibly too fast to be modelled with the current implementation of harmonic de-noising.

One possible approach to this issue could be to use differential measurements by separately measuring and compensating accordingly for these noise sources. This reference technique has been successfully applied in previous research, but only for few electrode combinations (Halverson et al., 1989; Radic, 2014).

5.1.2. Electromagnetic coupling

Electromagnetic coupling limits how close to the current switching point it is possible to use the DCIP data, limiting the spectral information content. Hardware improvements (such as cables or instruments) could possibly reduce some of the coupling effect. Other coupling sources (for example inductive) could be handled by keeping the affected data and by including the inductive coupling in the forward response and processing it in the inversion routine.

5.1.3. Data reliability at acquisition

The signal–processing scheme presented in this work is applied after the DCIP acquisition; thus, it is not possible to use the reliability measures during field acquisition. With real time processing (using more advanced or cloud connected instruments), it may be possible to use the data quality and reliability measures to automatically repeat failed measurements or to alert DCIP operators to possible issues, further enhancing the final data quality and reliability. This would possibly increase the survey time, but could also result in a more reliable and complete dataset after removal of erroneous data, increase the usefulness of the DCIP results, and reduce the time needed for data post–processing.

5.2. Survey time

5.2.1. Hardware

Instrumentation with more Tx and Rx channels would reduce the survey time further. Additionally, the possibility of using distributed (galvanically–separated) Tx and Rx instrumentation could facilitate logistics regarding deployment of measurement equipment at sites with restricted areas, for example surveys at different sides of major roads. Distributed systems would also increase the degree of freedom for electrode placements.

5.2.2. Dynamic waveform and protocol

The waveform time could possibly be further optimised regarding the pulse duration by dynamically adapting it to the desired subsurface information (spectral IP or only resistivity) and field conditions, such as noise and spectral response. Similarly, protocols could be dynamically optimised in the field for maximising SNR, sensitivity, lateral and vertical resolution for a predefined volume–of–interest, based on estimated electrical properties instead of based on a homogeneous half–space. With such a system, one or several subsurface volumes (or areas for 2D) could be defined for investigation, instead of defining a measurement protocol. Furthermore, additional electrode positions could be suggested in the field for further improving the information in the volume–of–interest.

5.3. Data post-processing

5.3.1. Automated data processing

Generally, spectral IP evaluation still demands large amounts of manual processing and filtering of erroneous data points before inversion is possible. With increasing data sets, and with typically thousands of electrode combinations and (for example) 40 IP gates per response, there is a need for automatic processing and filtering of the IP response data. Furthermore, recently developed methods only consider positive, strictly decaying IP responses as non-erroneous data, although other types of IP responses are physically possible. This calls for more advanced processing schemes, and could possibly be achieved by means of artificial intelligence. For example, machine learning together with continued research on what types of responses are physically possible.

6. References

- Argote-Espino, D., Tejero-Andrade, A., Cifuentes-Nava, G., Iriarte, L., Farías, S., Chávez, R.E., López, F., 2013. 3D electrical prospection in the archaeological site of El Pahñú, Hidalgo State, Central Mexico. *J. Archaeol. Sci.* 40, 1213–1223. <https://doi.org/10.1016/j.jas.2012.08.034>
- Auken, E., Doetsch, J., Fiandaca, G., Christiansen, A.V., Gazoty, A., Cahill, A.G., Jakobsen, R., 2014. Imaging subsurface migration of dissolved CO₂ in a shallow aquifer using 3-D time-lapse electrical resistivity tomography. *J. Appl. Geophys.* 101, 31–41. <https://doi.org/10.1016/j.jappgeo.2013.11.011>
- Auken, E., Pellerin, L., Christensen, N.B., Sørensen, K., 2006. A survey of current trends in near-surface electrical and electromagnetic methods. *Geophysics* 71, 249–260. <https://doi.org/10.1190/1.2335575>
- Binley, A., 2015. Tools and Techniques: Electrical Methods, in: *Treatise on Geophysics*. Elsevier, pp. 233–259. <https://doi.org/10.1016/B978-0-444-53802-4.00192-5>
- Butler, D.K., 2005. *Near-surface geophysics*. Society of Exploration Geophysicists Tulsa, ISBN: 1560801301.
- Dahlin, T., 2001. The development of DC resistivity imaging techniques. *Comput. Geosci.* 27, 1019–1029. [https://doi.org/10.1016/S0098-3004\(00\)00160-6](https://doi.org/10.1016/S0098-3004(00)00160-6)
- Dahlin, T., Bjelm, L., Svensson, C., 1999. Use of electrical imaging in site investigations for a railway tunnel through the Hallandsås Horst, Sweden. *Q. J. Eng. Geol. Hydrogeol.* 32, 163–173.
- Dahlin, T., Leroux, V., 2012. Improvement in time-domain induced polarization data quality with multi-electrode systems by separating current and potential cables. *Near Surf. Geophys.* 10, 545–656. <https://doi.org/10.3997/1873-0604.2012028>
- Dahlin, T., Leroux, V., Nissen, J., 2002. Measuring techniques in induced polarisation imaging. *J. Appl. Geophys.* 50, 279–298. [https://doi.org/10.1016/S0926-9851\(02\)00148-9](https://doi.org/10.1016/S0926-9851(02)00148-9)
- Dahlin, T., Rosqvist, H., Leroux, V., 2010. Resistivity-IP mapping for landfill applications. *First Break* 28.
- Dahlin, T., Zhou, B., 2006. Multiple-gradient array measurements for multichannel 2D resistivity imaging. *Near Surf. Geophys.* 4, 113–123. <https://doi.org/10.3997/1873-0604.2005037>
- Doetsch, J., Fiandaca, G., Auken, E., Christiansen, A.V., Cahill, A.G., 2015a. Field-scale time-domain spectral induced polarization monitoring of geochemical changes induced by

- injected CO₂ in a shallow aquifer. *Geophysics* 16, 10294. <https://doi.org/10.1190/geo2014-0315.1>
- Doetsch, J., Ingeman-Nielsen, T., Christiansen, A. V., Fiandaca, G., Auken, E., Elberling, B., Adamson, K., Lane, T., Elberling, B., 2015b. Direct current (DC) resistivity and induced polarization (IP) monitoring of active layer dynamics at high temporal resolution. *Cold Reg. Sci. Technol.* 119, 16–28. <https://doi.org/10.1016/j.coldregions.2015.07.002>
- Fetter, C.W., 2001. *Applied hydrogeology*. Prentice Hall, Upper Saddle River N.J., ISBN: 0131226878.
- Fiandaca, G., 2018. Induction-free acquisition range in spectral time- and frequency-domain induced polarization at field scale. *Geophys. J. Int.* <https://doi.org/10.1093/gji/ggy409>
- Fiandaca, G., Auken, E., Christiansen, A.V., Gazoty, A., 2012. Time-domain-induced polarization: Full-decay forward modeling and 1D laterally constrained inversion of Cole-Cole parameters. *Geophysics* 77, E213–E225. <https://doi.org/10.1190/geo2011-0217.1>
- Fiandaca, G., Maurya, P.K., Balbarini, N., Hördt, A., Christiansen, A. V., Foged, N., Bjerg, P.L., Auken, E., 2018. Permeability Estimation Directly From Logging-While-Drilling Induced Polarization Data. *Water Resour. Res.* 54, 2851–2870. <https://doi.org/10.1002/2017WR022411>
- Fiandaca, G., Olsson, P.-I., Maurya, P.K., Kühn, A., Bording, T.S., Dahlin, T., Auken, E., 2019. Non-Standard Responses in Time-Domain Induced Polarization Measurements. <https://doi.org/10.3997/2214-4609.201902360>
- Fiandaca, G., Ramm, J., Binley, A., Gazoty, A., Christiansen, A.V., Auken, E., 2013. Resolving spectral information from time domain induced polarization data through 2-D inversion. *Geophys. J. Int.* 192, 631–646. <https://doi.org/10.1093/gji/ggs060>
- Fink, J.B., 1990. *Induced polarization: applications and case histories*. Soc of Exploration Geophysicists, ISBN: 0931830893.
- Flores Orozco, A., Gallistl, J., Bücker, M., Williams, K.H., 2018. Decay curve analysis for data error quantification in time-domain induced polarization imaging. *Geophysics* 83, E75–E86. <https://doi.org/10.1190/geo2016-0714.1>
- Florsch, N., Llubes, M., Téreygeol, F., Ghorbani, A., Roblet, P., 2011. Quantification of slag heap volumes and masses through the use of induced polarization: application to the Castel-Minier site. *J. Archaeol. Sci.* 38, 438–451. <https://doi.org/10.1016/j.jas.2010.09.027>
- Gazoty, A., Fiandaca, G., Pedersen, J., Auken, E., Christiansen, A.V., 2013. Data repeatability and acquisition techniques for time-domain spectral induced polarization. *Near Surf. Geophys.* 11, 391–406. <https://doi.org/10.3997/1873-0604.2013013>
- Gazoty, A., Fiandaca, G., Pedersen, J., Auken, E., Christiansen, A. V., Pedersen, J.K., 2012a. Application of time domain induced polarization to the mapping of lithotypes in a landfill site. *Hydrol. Earth Syst. Sci.* 16, 1793–1804. <https://doi.org/10.5194/hess-16-1793-2012>
- Gazoty, A., Fiandaca, G., Pedersen, J., Auken, E., Christiansen, A. V., 2012b. Mapping of

- landfills using time-domain spectral induced polarization data: The Eskelund case study. *Near Surf. Geophys.* 10, 575–586. <https://doi.org/10.3997/1873-0604.2012046>
- Glover, P.W.J., 2015. *Geophysical Properties of the Near Surface Earth: Electrical Properties, Treatise on Geophysics*. Elsevier B.V., ISBN: 9780444538024. <https://doi.org/10.1016/B978-0-444-53802-4.00189-5>
- Hallbauer-Zadorozhnaya, V., Santarato, G., Abu Zeid, N., 2015. Non-linear behaviour of electrical parameters in porous, water-saturated rocks: A model to predict pore size distribution. *Geophys. J. Int.* 202, 871–886. <https://doi.org/10.1093/gji/ggv161>
- Hönig, M., Tezkan, B., 2007. 1D and 2D Cole-Cole-inversion of time-domain induced-polarization data. *Geophys. Prospect.* 55, 117–133. <https://doi.org/10.1111/j.1365-2478.2006.00570.x>
- Ingeman-Nielsen, T., Baumgartner, F., 2006. Numerical modelling of complex resistivity effects on a homogenous half-space at low frequencies. *Geophys. Prospect.* 54, 261–271. <https://doi.org/10.1111/j.1365-2478.2006.00532.x>
- Johansson, S., Sparrenbom, C., Fiandaca, G., Lindskog, A., Olsson, P.-I., Dahlin, T., Rosqvist, H., 2017. Investigations of a Cretaceous limestone with spectral induced polarization and scanning electron microscopy. *Geophys. J. Int.* 208, 954–972. <https://doi.org/10.1093/gji/ggw432>
- Johnson, I.M., 1984. Spectral induced polarization parameters as determined through time-domain measurements. *Geophysics* 49, 1993–2003. <https://doi.org/10.1190/1.1441610>
- Kang, S., Oldenburg, D.W., 2018. Time domain electromagnetic-induced polarisation: extracting more induced polarisation information from grounded source time domain electromagnetic data. *Geophys. Prospect.* 66, 74–86. <https://doi.org/10.1111/1365-2478.12600>
- Kemna, A., Binley, A., Slater, L., 2004. Crosshole IP imaging for engineering and environmental applications. *Geophysics* 69, 97–107. <https://doi.org/10.1190/1.1649379>
- Lajaunie, M., Maurya, P.K., Fiandaca, G., 2016. Comparison of Cole-Cole and Constant Phase Angle modeling in Time-Domain Induced Polarization, in: *Proceedings of the 4th International Workshop on Induced Polarization*. Aarhus, Denmark.
- Leroux, V., Dahlin, T., 2005. Time-lapse resistivity investigations for imaging saltwater transport in glaciofluvial deposits. *Environ. Geol.* 49, 347–358. <https://doi.org/10.1007/s00254-005-0070-7>
- Leroux, V., Dahlin, T., Svensson, M., 2007. Dense resistivity and induced polarization profiling for a landfill restoration project at Härlov, Southern Sweden. *Waste Manag. Res.* 25, 49–60. <https://doi.org/10.1177/0734242X07073668>
- Loke, M.H., Barker, R.D., 1996. Practical techniques for 3D resistivity surveys and data inversion1. *Geophys. Prospect.* 44, 499–523. <https://doi.org/10.1111/j.1365-2478.1996.tb00162.x>
- Loke, M.H., Chambers, J.E., Rucker, D.F., Kuras, O., Wilkinson, P.B., 2013. Recent developments in the direct-current geoelectrical imaging method. *J. Appl. Geophys.* 95,

- 135–156. <https://doi.org/10.1016/j.jappgeo.2013.02.017>
- Madsen, L.M., Fiandaca, G., Auken, E., Christiansen, A.V., 2017. Time-domain induced polarization – an analysis of Cole–Cole parameter resolution and correlation using Markov Chain Monte Carlo inversion. *Geophys. J. Int.* 211, 1341–1353. <https://doi.org/10.1093/gji/ggx355>
- Madsen, L.M., Fiandaca, G., Christiansen, A.V., Auken, E., 2018. Resolution of well-known resistivity equivalences by inclusion of time-domain induced polarization data. *Geophysics* 83, E47–E54. <https://doi.org/10.1190/geo2017-0009.1>
- Maurya, P.K., Balbarini, N., Møller, I., Rønde, V., Christiansen, A. V, Bjerg, P.L., Auken, E., Fiandaca, G., 2018a. Subsurface imaging of water electrical conductivity, hydraulic permeability and lithology at contaminated sites by induced polarization. *Geophys. J. Int.* 213, 770–785. <https://doi.org/10.1093/gji/ggy018>
- Maurya, P.K., Fiandaca, G., Christiansen, A. V, Auken, E., 2018b. Field-scale comparison of frequency- and time-domain spectral induced polarization. *Geophys. J. Int.* 214, 1441–1465. <https://doi.org/10.1093/gji/ggy218>
- Maurya, P.K., Rønde, V.K., Fiandaca, G., Balbarini, N., Auken, E., Bjerg, P.L., Christiansen, A.V., 2017. Detailed landfill leachate plume mapping using 2D and 3D electrical resistivity tomography - with correlation to ionic strength measured in screens. *J. Appl. Geophys.* 138, 1–8. <https://doi.org/10.1016/J.JAPPGEO.2017.01.019>
- McGillivray, P.R., Oldenburg, D.W., 1990. Methods for calculating frechet derivatives and sensitivities for the non-linear inverse problem: a comparative study1. *Geophys. Prospect.* 38, 499–524. <https://doi.org/10.1111/j.1365-2478.1990.tb01859.x>
- Nijland, W., van der Meijde, M., Addink, E.A., de Jong, S.M., 2010. Detection of soil moisture and vegetation water abstraction in a Mediterranean natural area using electrical resistivity tomography. *CATENA* 81, 209–216. <https://doi.org/10.1016/j.catena.2010.03.005>
- Olsson, P.-I., 2016. Optimization of time domain induced polarization data acquisition and spectral information content, (Licentiate Thesis). Lund University, Lund, ISBN: 9789176236727.
- Olsson, P.-I., Dahlin, T., Fiandaca, G., Auken, E., 2015. Measuring time-domain spectral induced polarization in the on-time: decreasing acquisition time and increasing signal-to-noise ratio. *J. Appl. Geophys.* 123, 316–321. <https://doi.org/10.1016/j.jappgeo.2015.08.009>
- Olsson, P.-I., Fiandaca, G., Larsen, J.J., Dahlin, T., Auken, E., 2016. Doubling the spectrum of time-domain induced polarization by harmonic de-noising, drift correction, spike removal, tapered gating and data uncertainty estimation. *Geophys. J. Int.* 207, 774–784. <https://doi.org/10.1093/gji/ggw260>
- Olsson, P.-I., Fiandaca, G., Maurya, P.K., Dahlin, T., Auken, E., 2019. Effect of current pulse duration in recovering quantitative induced polarization models from time-domain full-response and integral chargeability data. *Geophys. J. Int.* 218, 1739–1747. <https://doi.org/10.1093/gji/ggz236>

- Olsson, P.-I., Jonsson, P., Johansson, S., Johansson, L., 2017. BeFo 382 - Detailed Comparison Study of 3D-characterized Rock Mass and Geophysical Models, in: *Near Surface Geoscience 2017 - 23rd European Meeting of Environmental and Engineering Geophysics*. Malmö, Sweden. <https://doi.org/10.3997/2214-4609.201702005>
- Pelton, W.H., Ward, S.H., Hallof, P.G., Sill, W.R., Nelson, P.H., 1978. Mineral discrimination and removal of inductive coupling with multifrequency IP. *Geophysics* 43, 588–609. <https://doi.org/10.1190/1.1440839>
- Peter-Borie, M., Sirieix, C., Naudet, V., Riss, J., 2011. Electrical resistivity monitoring with buried electrodes and cables: noise estimation with repeatability tests. *Near Surf. Geophys.* 9, 369–380. <https://doi.org/10.3997/1873-0604.2011013>
- Radic, T., 2004. Elimination of Cable Effects while Multi-Channel SIP Measurements, in: *Near Surface 2004 - 10th EAGE European Meeting of Environmental and Engineering Geophysics*. Utrecht, The Netherlands, pp. 1–4.
- Revil, A., Binley, A., Mejus, L., Kessouri, P., 2015. Predicting permeability from the characteristic relaxation time and intrinsic formation factor of complex conductivity spectra. *Water Resour. Res.* 51, 6672–6700. <https://doi.org/10.1002/2015WR017074>
- Rossi, M., Dahlin, T., Olsson, P.-I., Günther, T., 2018. Data acquisition, processing and filtering for reliable 3D resistivity and time-domain induced polarisation tomography in an urban area: field example of Vinsta, Stockholm. *Near Surf. Geophys.* 16, 220–229. <https://doi.org/10.3997/1873-0604.2018014>
- Rossi, M., Olsson, P.-I., Johansson, S., Fiandaca, G., Preis Bergdahl, D., Dahlin, T., 2017. Mapping geological structures in bedrock via large-scale direct current resistivity and time-domain induced polarization tomography. *Near Surf. Geophys.* 15, 657–667. <https://doi.org/10.3997/1873-0604.2017058>
- Rücker, C., Günther, T., Spitzer, K., Rücker, C., Spitzer, K., 2006. Three-dimensional modelling and inversion of dc resistivity data incorporating topography - I. Modelling. *Geophys. J. Int.* 166, 495–505. <https://doi.org/10.1111/j.1365-246X.2006.03011.x>
- Seigel, H.O., 1959. Mathematical formulation and type curves for induced polarization. *Geophysics* 24, 547–565. <https://doi.org/10.1190/1.1438625>
- Slater, L., Ntarlagiannis, D., Yee, N., O'Brien, M., Zhang, C., Williams, K.H., 2008. Electrodeic voltages in the presence of dissolved sulfide: Implications for monitoring natural microbial activity. *Geophysics* 73, F65–F70. <https://doi.org/10.1190/1.2828977>
- Slater, L.D., Glaser, D.R., 2003. Controls on induced polarization in sandy unconsolidated sediments and application to aquifer characterization. *Geophysics* 68, 1547. <https://doi.org/10.1190/1.1620628>
- Slater, L.D., Lesmes, D., 2002. IP interpretation in environmental investigations. *Geophysics* 67, 77–88. <https://doi.org/10.1190/1.1451353>
- Stummer, P., Maurer, H., Horstmeyer, H., Green, A.G., 2002. Optimization of DC resistivity data acquisition: real-time experimental design and a new multielectrode system. *IEEE Trans. Geosci. Remote Sens.* 40, 2727–2735.

<https://doi.org/10.1109/TGRS.2002.807015>

- Sumner, J.S., 1976. Principles of induced polarization for geophysical exploration. Elsevier, ISBN: 0444599878.
- Tombs, J.M.C., 1981. The feasibility of making spectral IP measurements in the time domain. *Geoexploration* 19, 91–102. [https://doi.org/10.1016/0016-7142\(81\)90022-3](https://doi.org/10.1016/0016-7142(81)90022-3)
- Yamashita, Y., Lebert, F., Gourry, J.C., Bourgeois, B., Texier, B., 2014. Time-domain Induced Polarization Profile with Multiple-current Transmission, in: *Near Surface Geoscience 2014 - 20th European Meeting of Environmental and Engineering Geophysics*. Athens, Greece, pp. 1–5. <https://doi.org/10.3997/2214-4609.20141985>
- Zonge, K., Wynn, J., Urquhart, S., 2005. 9. Resistivity, Induced Polarization, and Complex Resistivity, in: *Near-Surface Geophysics*. Society of Exploration Geophysicists, pp. 265–300. <https://doi.org/10.1190/1.9781560801719.ch9>



Box 5501
SE-114 85 Stockholm

info@befoonline.org • www.befoonline.org
Visiting address: Storgatan 19, Stockholm

ISSN 1104-1773